JOURNAL OF GEOPHYSICAL RESEARCH, VOL. 106, NO. C9, PAGES 19,809–19,824, SEPTEMBER 15, 2001

Impact of variable inflow on the dynamics of a coastal buoyant plume

Alexander E. Yankovsky

Nova Southeastern University Oceanographic Center, Dania Beach, Florida, USA

Barbara M. Hickey

School of Oceanography, University of Washington, Seattle, Washington, USA

Andreas K. Münchow

College of Marine Studies, University of Delaware, Newark, Delaware, USA

Abstract. The impact of buoyant discharge variations on the dynamics of coastal buoyancy-driven currents is studied using a primitive equation numerical model (SPEM5). First, variable discharge is introduced as harmonic fluctuations of the inflow velocity at the tidal (period 12 hours) and subinertial (period 10 days) frequencies. Tidal fluctuations produce only minor effects on the buoyant plume compared to the case of constant inflow, while subinertial fluctuations substantially modify the anticyclonic bulge. A partially detached anticyclonic plume forms when discharge subsides after reaching its peak value. Such a plume has maximum offshore extension some distance downstream of the mouth with the lightest water separated from the coast. A secondary bulge forms during the low runoff interval. When high discharge resumes, this secondary bulge is shifted offshore and enhanced for some time. An individual high-discharge event is next considered, where both the net transport of the inflow and the absolute value of its density anomaly increase and then return to their initial (background) values over 5 and 10 day time intervals. This event also generates a partially detached plume (especially with the 10 day duration). In this case, the lightest water occupies the downstream part of the bulge and is separated not only from the coast but also from the mouth. The effect of variable discharge is more dramatic with a uniform downstream current of 0.1 m s^{-1}. Under such conditions, constant buoyant discharge does not form a well-pronounced anticyclonic bulge. In contrast, variable discharge produces an almost circular anticyclone during the high-runoff interval. As runoff decreases, this anticyclone separates from the source and either continues to propagate downstream as an individual eddy or is modified by the next cycle of increasing discharge. Observational evidence for both the partially detached bulge near the mouth and the anticyclone propagating downstream from its source is presented in this study. One feature was observed at the mouth of the Columbia River estuary; the second feature was observed off the southern New Jersey coast ~ 150 km south of its source, the Hudson estuary.

1. Introduction

Buoyancy forcing plays a major role and in most cases is only inferior to wind stress forcing with respect to the subinertial dynamics of the coastal ocean. While subinertial variability of wind forcing has been the subject of numerous papers (see the list of references in the review by Brink [1991]), process-oriented studies of buoyancy-driven currents have typically assumed constant inflow [e.g., *Chao*, 1988; *Oey and Mellor*, 1993; *Yankovsky and Chapman*, 1997; *Garvine*, 1999]. Rossby adjustment-type studies on the setup of a buoyant plume after the release of light water have also been made [*Chao and Boicourt*, 1986; *Weaver and Hsieh*, 1987]. Although these latter authors emphasized transient or nonstationary components in the plume's dynamics, they essentially concentrated on the formation of the plume and also on its relaxation after the buoyant forcing ceased [also see *Chao*, 1988; *Valle-Levinson et al.*, 1996].

Thus the influence of a continuous but variable discharge on the dynamics of an existing (that is, already formed) plume has not been addressed. Variability in buoyant inflow at the mouth of an estuary can be caused by variable river discharge, by variable estuarine mixing due to tidal or wind forcing, and by the direct action of wind stress. Most studies that did include subinertial variability of discharge were attempts to simulate a specific buoyancy-driven flow and, as such, considered the coastal ocean in all its complexity [i.e., *Kourafalou et al.*, 1996; *Masson and Cummins*, 1999]. This complexity obscured the consequence of discharge variability on the structure and dynamics of the buoyancy-driven current.

Recent observational studies of buoyancy-driven currents have delineated many robust features not seen previously in numerical models. For example, observations on the New Jersey shelf in summer 1996 [*Yankovsky et al.*, 2000]

Paper number 2001JC000792.
0148-0227/01/2001JC000792$09.00

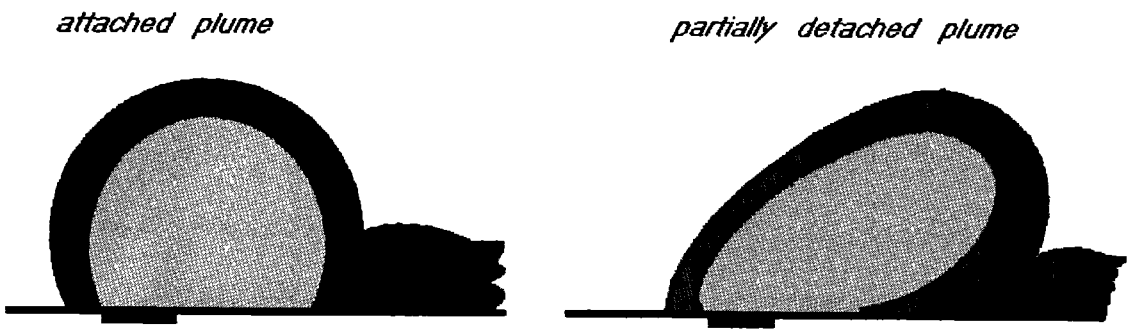

Figure 1. Schematic of the attached and partially detached anticyclonic bulges. The light-shaded area is the core of the plume filled with buoyant water; the darker area is a frontal zone. The bar indicates buoyancy source.

revealed that the Hudson Coastal Current did not always form a band of light water downstream along the coast as numerical models would suggest. Hereinafter, we define the downstream direction as the direction of the Kelvin wave propagation. Instead, bulges of buoyant water episodically propagated through the study domain. Similar features were observed off New Jersey in summer 1989 [*Münchow*, 1992].

Observations of the Columbia River plume near its source region in winter 1990-1991 demonstrated that in some cases the anticyclonic bulge was partially detached from the coast [*Hickey et al.*, 1998]. In such cases the plume had two distinctive features: (1) the bulge was swept downstream so that the maximum offshore extension of the bulge occurred downstream from the source and (2) at the location of this maximum offshore extension, the lightest water in the bulge was separated from the coast. Figure 1 shows a schematic of a partially detached anticyclonic bulge as defined above. The definition is motivated by the Columbia River plume observations and will be applied to our model results as well. For comparison, Figure 1 also shows a bulge attached to the coast. The latter is usually produced in numerical models with constant buoyant inflow. The instantaneous structure of the Columbia River plume strongly depends on the local wind stress so that a variety of anticyclonic bulge patterns was observed [*Hickey et al.*, 1998]. Nevertheless, the partially detached bulge structure described above was sufficiently robust to appear as the leading mode in an empirical orthogonal function (EOF) analysis of the salinity time series [*Hickey et al.*, 1998].

As the examples of the Columbia River plume and the Hudson Coastal Current show, both the source region and the downstream buoyancy-driven current exhibit features absent in earlier process-oriented studies. This suggests missing physics in prior models. Here we address the impact of variable discharge on the dynamics of a buoyant plume as a possible cause for the observed phenomena.

Sugimoto [1990] discussed observational evidence for 25 day fluctuations in the Tsugaru Warm Gyre. These fluctuations included an offshore extension of the gyre, its detachment from the coast, as well as the southward (i.e., downstream) spreading, and splitting of the gyre. These features were caused by variations of warm water outflow from Tsugaru Strait and were also reproduced in laboratory experiments with variable discharge. Although the Tsugaru Warm Gyre has a larger spatial scale than the typical river plume, these results demonstrate the significant impact that subinertial variability of buoyant inflow can have on coastal buoyant current dynamics.

In this study, we will introduce variable discharge and (in some cases) uniform ambient current on the shelf while retaining a fairly simple model configuration. Section 2 describes the model configuration. Section 3 presents the results of model experiments and explains the effect of discharge variability on the plume's structure and dynamics. Section 4 addresses the observations of the Columbia River plume and the Hudson Coastal Current relevant to this study, while section 5 concludes and summarizes the paper.

2. Numerical Model

The SPEM5.1 primitive equation numerical model is used in our study. This is an improved and modified version of the model originally described by *Haidvogel et al.* (1991). The model solves the nonlinear momentum and mass balance equations based on the rigid lid, Boussinesq, f plane and hydrostatic approximations:

$$u_t + \mathbf{v} \bullet \nabla u - fv = -\frac{1}{\rho_0} p_x + (A_v u_z)_z + F_u , \quad (1)$$

$$v_t + \mathbf{v} \bullet \nabla v + fu = -\frac{1}{\rho_0} p_y + (A_v v_z)_z + F_v , \quad (2)$$

$$p_z = -g\rho , \quad (3)$$

$$\nabla \bullet \mathbf{v} = 0 , \quad (4)$$

$$\rho_t + \mathbf{v} \bullet \nabla \rho = (K_v \rho_z)_z + F_\rho . \quad (5)$$

Here $\mathbf{v}$ is the velocity vector with u, v, w components along the x, y, z coordinates; ρ is the density difference from the constant reference density of the ambient flow ρ_0=1020 kg m^{-3}; p is the pressure; $f = 10^{-4}$ s^{-1} is the Coriolis parameter and g is the acceleration due to gravity. The subscripts t, x, y, z denote partial differentiation with respect to time and spatial coordinates. The coefficients for vertical eddy viscosity, A_V, and diffusivity, K_V, are parameterized using the Mellor-Yamada 2.0 closure scheme [*Mellor and Yamada*, 1974]. Terms F_u, F_v, and F_ρ represent the effect of dissipation required for numerical stability.

The model domain is a channel bounded by two parallel vertical walls (Figure 2, top). The shallower coastal wall of depth h_0=15 m coincides with the x coordinate while the y

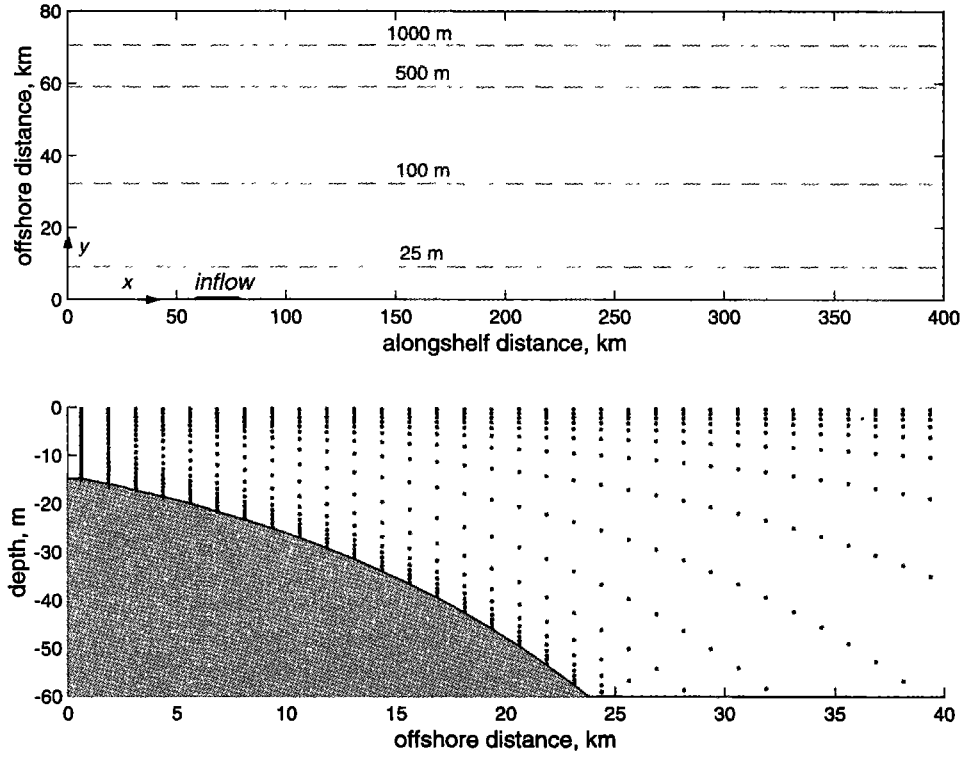

Figure 2. Model domain: (top) plan view and (bottom) across-shelf transect showing the vertical grid spacing (only the top 60 m of the domain are shown).

coordinate is directed offshore. The depth h varies exponentially in the y (offshore) direction:

$$h = h_0 e^{\lambda y}, \tag{6}$$

where λ=6 10^{-5} m^{-1}. The model bottom slope changes from 0.001 to 0.004 within 20 km from the coast (Figure 2 bottom). These numbers give a reasonable range of values compared to actual shelves: The first number is typical for the Mid-Atlantic Bight shelf, while the second represents the Washington shelf. We will model a surface-advected plume with the buoyant layer spreading very near the surface [*Yankovsky and Chapman*, 1997]. Thus the influence of bottom slope will be limited to 15-20 km offshore distance where the plume detaches but still interacts with the bottom; see Figure 16 (left) by [*Yankovsky*, 2000] as an example of a similar plume. The exponential depth profile is required in order to introduce a waveguide for subinertial coastally trapped waves. This, in turn, will allow realistic speeds for downstream propagation of the energy associated with the subinertial transients generated by the variable inflow. The channel's width is 80 km.

The across-channel boundaries are at x=0 and 400 km where the open boundary conditions discussed below are applied. The numerical grid is rectangular in the horizontal, with uniform grid spacing in both directions: Δ_x=2.5 km (161 grid cells in x) and Δ_y=1.25 km (65 grid cells in y). The coarser resolution in the x coordinate is based on the assumption that alongshelf scales in the coastal ocean tend to exceed across-shelf scales for mesoscale and larger-scale dynamics. However, in the case of a buoyant plume the gradients can be comparable in both directions, especially in the bulge region. The sensitivity of the numerical solution to the alongshelf resolution was tested by repeating a standard case (see below) with Δ_x=1.75 km. The results were identical. The generalized s coordinate is applied in the vertical [*Song and Haidvogel*, 1994], with high vertical resolution in the dynamically important surface and bottom layers and a stretched (topography following) coordinate in the interior. We use 18 grid cells in the vertical (Figure 2, bottom). The model time step is 600 s.

A rigid lid is assumed at the surface, and no normal flow is allowed through the bottom and walls, with the exception for the buoyant discharge through the coastal wall which forces the model. A buoyant inflow is specified through the gap with the upstream edge located at x=60 km and the gap width set to L=10 km. The inflow has spatially uniform but time-varying velocity v_i and density anomaly ρ_i. The walls are slippery (no stress), while the bottom is frictional, and the stress is specified using a linear bottom friction parameterization,

$$A_v u_z = ru \quad A_v v_z = rv \quad z=-h, \tag{7}$$

where r=2.65 10^{-4} m s^{-1} is the bottom friction coefficient. The background (minimum) values of the vertical viscosity and diffusivity coefficients in the Mellor-Yamada closure scheme are set to 2 10^{-5} m^2 s^{-1}. Dissipative functions F_u, F_v, and F_ρ are applied in the form of lateral Laplacian mixing along the s coordinate surfaces with a constant mixing coefficient of 20 m^2 s^{-1}.

Since the discharge propagates downstream (in the positive x direction), we apply a radiation boundary condition for depth-averaged velocity components [*Yankovsky and Chapman*, 1997; *Chapman and Lentz*, 1994]. This condition assumes that the vorticity of the depth-

averaged velocity propagates through the open boundary at a constant speed. A "smooth" condition (zero x derivative) is applied to the depth-varying quantities at both upstream and downstream open boundaries.

Initially, the water in the domain is either quiescent or flows downstream at a uniform speed of 0.1 m s^{-1} with a constant density anomaly of ρ=0. The model is then forced by the prescribed buoyant inflow. The duration of model runs varies from 20 to 30 days.

3. Results

3.1. Harmonic Buoyant Inflow

We start with the case of discharge varying in time as a harmonic function. We will compare these model runs against the case with constant discharge (hereinafter referred to as the standard case, or model run 1). For the constant discharge case, inflow velocity v_i is 0.15 m s^{-1}. The variable discharge is specified as

$$v_i = 0.15[1-\cos(\omega t)] \quad (8)$$

where $\omega=2\pi/T$ is the frequency of the inflow oscillations, while T is their period. For the standard case, the discharge rate is 2.25 10^4 m^3 s^{-1}, while for the variable inflow the rate varies from 0 to 4.5 10^4 m^3 s^{-1}. The net transport of buoyant water into the domain over one period of the inflow oscillation is equal to the net transport in the case of constant inflow over the same time interval. In all cases, the density anomaly ρ_i is set to -3 kg m^{-3}. We apply a buoyant forcing typical of inflow from an estuary. Thus the density anomaly is smaller than for direct river discharge on the shelf, while the net transport is larger. Both properties result from the estuarine mixing of the river and oceanic waters.

The baroclinic Rossby radius ($Rd = \sqrt{g'h_0}/f$, where $g' = g\,|\Delta\rho|/\rho_0$) of the inflow is 6.58 km. The corresponding Burger number of the inflow is $S = Rd/L$ =0.66, and the Froude number is $F = v_i/\sqrt{g'h_0}$ =0.23. The chosen inflow parameters introduce a moderately large midlatitude plume which is typically subcritical (F<1) and is strongly affected by the Earth's rotation (S<1) [*Garvine*, 1995]. Examples of such systems include discharges from the Chesapeake and Delaware Bay and Hudson estuary into the Mid-Atlantic Bight, the Columbia River inflow onto the Washington shelf, the Rhine and Dnepr River discharges into the North and Black Sea, respectively.

Two periodic fluctuations will be considered next; i.e., T=0.5 days (model run 2) and T=10 days (model run 3) representing tidal and subinertial variability of the inflow, respectively (Figure 3a). The case with tidal variability is not intended to model interaction between the plume and tidal currents. Such interaction, through mixing, can significantly influence buoyant current, limiting its offshore and downstream penetration [*Garvine*, 1999] or even periodically altering the stratification of buoyant plume [*Simpson and Souza*, 1995]. Although important to shelf dynamics, these features are beyond the scope of this paper. Instead, we will concentrate solely on a single physical process, i.e., the consequence of buoyant inflow temporal variability.

Anticyclonic bulges in numerical models with quiescent ambient flow tend to grow infinitely if they are not affected by bottom friction and do not interact with bottom topography [*Fong*, 1998; *Garvine*, 2001; *Nof and Pichevin*, 2001]. *Nof and Pichevin* [2001] offer an explanation for this phenomena based on the imbalance of the alongshelf momentum flux [see also *Pichevin and Nof*, 1997]. To illustrates this behavior, the temporal evolution of the net downstream transport around the anticyclonic bulge

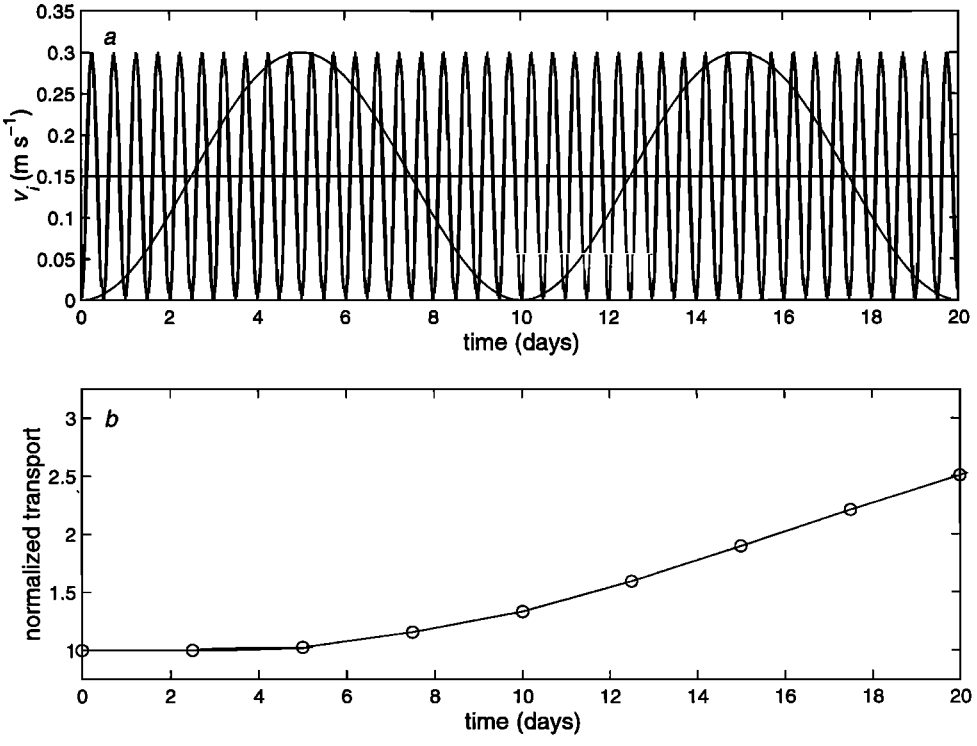

Figure 3. Temporal evolution of (a) the inflow velocity v_i in model runs 1-3 and (b) the net downstream transport around the bulge normalized by the net inflow transport in model run 1.

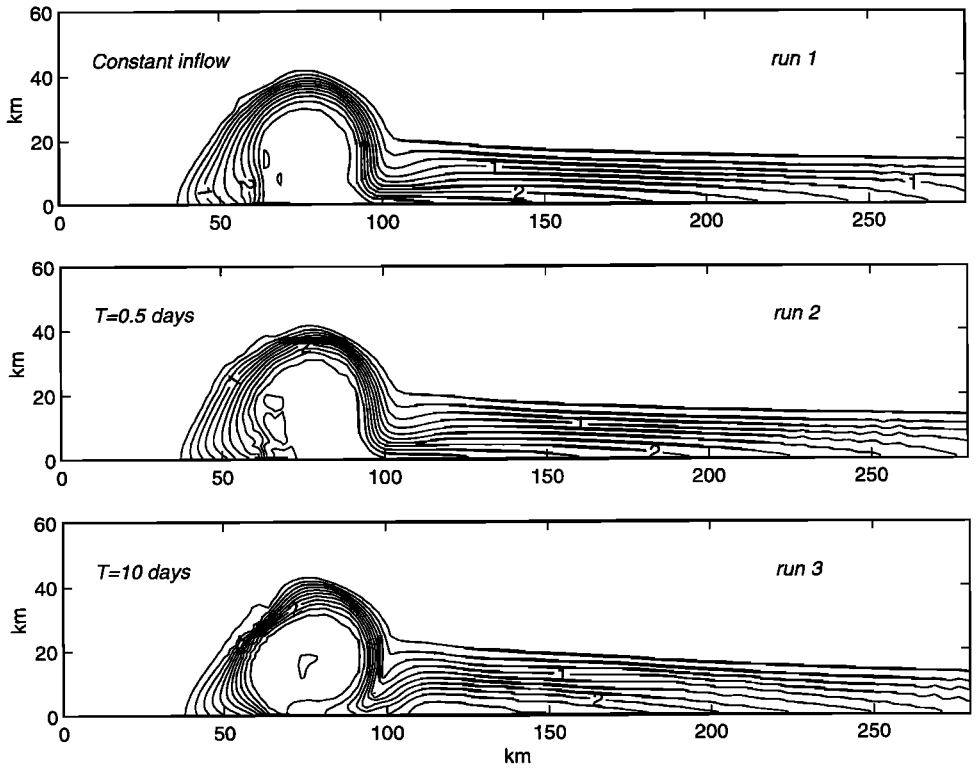

Figure 4. Absolute value of the density anomaly at the surface on day 20 with a contour interval of 0.25 kg m^{-3} for model runs 1-3.

normalized by the inflow transport (which is held constant) is shown for the standard case (Figure 3b). For this estimation we use the maximum value of the integral streamfunction in the center of the anticyclonic bulge normalized by the maximum streamfunction value at the mouth. After 10 days the net transport around the bulge grows linearly in time.

The large amount of buoyant water recirculating around the bulge, several times greater than the net (average) discharge, appears unrealistic. For this reason, we limit the duration of our model runs without a mean shelf current to 20 days. Continuous growth of the anticyclonic bulge with time is reduced with a decrease of coastal wall depth [*Garvine*, 2001]. *Chapman* [2000] found that ambient stratification also arrests the growth of the anticyclonic bulge at the surface. Furthermore, the growth of the anticyclonic bulge is highly susceptible to ambient currents on the shelf which are almost always present in the real coastal ocean. Even a weak downstream ambient flow arrests the offshore growth of the plume at the source [*Fong*, 1998], while a weak upstream flow causes a periodic shedding of almost circular anticyclones which subsequently drift upstream with the mean current [*Yankovsky*, 2000]. Both the offshore growth of the bulge and the downstream penetration of the buoyancy-driven coastal current are smaller in the real ocean. This suggests more efficient mixing or dispersion of buoyant flow in nature than in numerical models. These arguments justify ignoring the later stages of bulge growth in model runs.

Figure 4 shows surface density fields on day 20 for the three different buoyant discharges: constant inflow (model run 1, top), inflow varying with a 0.5 day period (model run 2, middle) and inflow varying with a 10 day period (model run 3, bottom). The plume in the standard case (run 1) is similar to its counterpart shown in Figure 3 by *Yankovsky* [2000]. The latter was obtained with a linear depth profile. This confirms our assumption that the surface-advected plume forced by constant inflow is relatively insensitive to the dramatic increase in bottom slope farther offshore (exponential depth profile). The anticyclonic bulges look similar in the standard and tidal cases. On the other hand, subinertial variability of the inflow (model run 3) forms a partially detached plume as defined in section 1. Indeed, the maximum offshore extension of the anticyclone's core (filled with the lightest water) is shifted slightly downstream compared with the standard case. At the same time, heavier water penetrates between the coastal wall and the center of the anticyclone at the location of its maximum offshore extension. In the upstream part the bulge has a sharper frontal zone which appears almost like a straight line tilted downsteam. The bulge is partly detached because the heavier water is advected anticyclonically toward the coast in its downstream segment and, upon reaching the coastal wall, continues farther upstream.

Figure 5 shows integral streamfunctions and surface density fields in model run 3 over a 10 day period spanning the time interval between two maxima in buoyant water discharge. On day 7.5 the inflow subsides by 50%, having reached its maximum on day 5. At the same time, downstream transport within the bulge remains at the higher level set up during the maximum discharge on day 5. As a result, closed streamlines are formed within the bulge with the upstream flow near the coast compensating for the abrupt reduction in the inflow rate. This tendency continues through day 10 when the discharge ceases and a closed anticyclonic circulation forms around the bulge. Denser water is advected

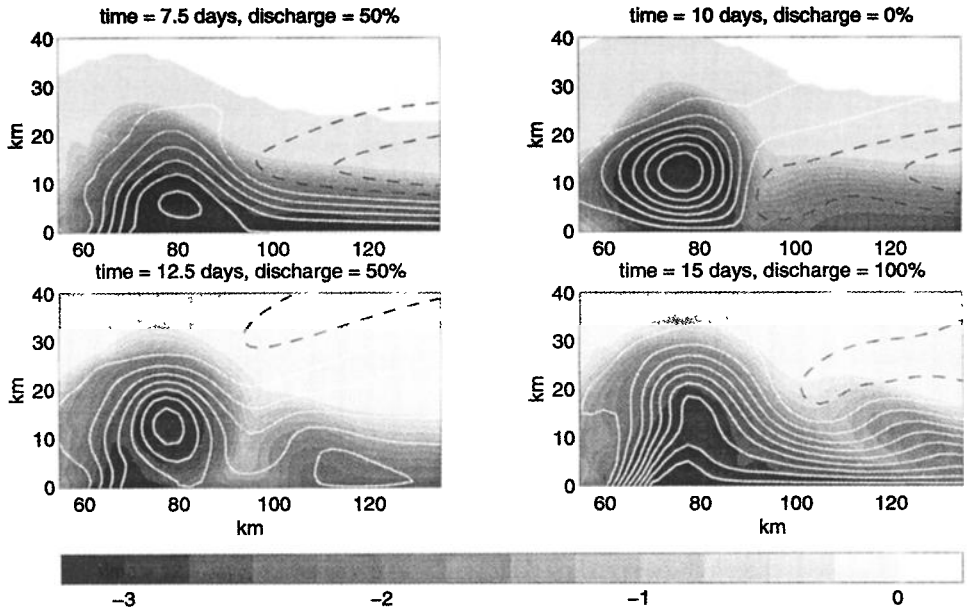

Figure 5. Model run 3. Density anomaly at the surface and integral stream function (solid contours are positive, dashed contours are negative; contour interval is 5 10^3 m^3 s^{-1}) at four different times during a 10 day cycle of discharge variation.

toward the coast along the downstream edge of the anticyclone. This terminates the continuous band of the lightest water near the coast in the range $90<x<105$ km (Figure 5, day 10). The separation of the lightest water in the bulge and in the downstream coastal current results in the formation of a secondary bulge or anticyclone at x=100-120 km on day 10-12.5. When the discharge resumes, the anticyclonic circulation around the bulge still dominates the dynamics near the source for some time: On day 12.5 discharged buoyant water turns slightly upstream and then flows around the anticyclone. The newly discharged water remains separated from the "old" lightest water in the center of the anticyclone (Figure 5, day 12.5). In the downstream part of the anticyclone, penetration of denser water toward the coast and then upstream continues. The gap between the lightest water in the bulge and in the downstream coastal current widens with the formation of closed streamlines in the secondary bulge. Only when the discharge regains its maximum strength on day 15 does recirculation in the bulge cease. Streamlines originating from the mouth turn to the right, continue through the bulge and completely suppress closed streamlines associated with the anticyclone. The secondary bulge is shifted offshore by the enhanced current at the wall because of higher discharge. There is no "discontinuity" in the surface density field between the anticyclonic bulge and the downstream coastal current.

The variable discharge causes uneven growth of the bulge depending on the particular phase of the inflow cycle (Figure 6). Here we show the temporal evolution of the -1.5 kg m^{-3} density contour representing the position of the front separating buoyant and ambient waters. From day 5 through day 7.5, during high but subsiding runoff, the bulge grows mainly in its downstream part. From day 7.5 through day 10, during low runoff, the bulge radially advances in its upstream and central parts but retreats in its downstream segment. From day 10 through day 12.5 the bulge continues to advance laterally in all directions except at its downstream edge where the isopycnal -1.5 kg m^{-3} almost reaches the

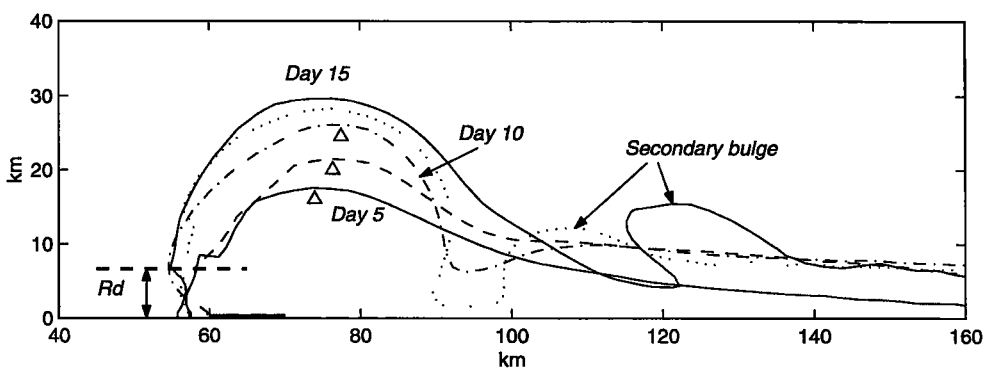

Figure 6. Model run 3. Location of the density anomaly contour −1.5 kg m^{-3} at the surface is shown at 2.5 day intervals from day 5 through day 15. Triangles indicate the maximum offshore extension of the bulge. The heavy dashed line indicates the offshore scale of the baroclinic Rossby radius, *Rd*.

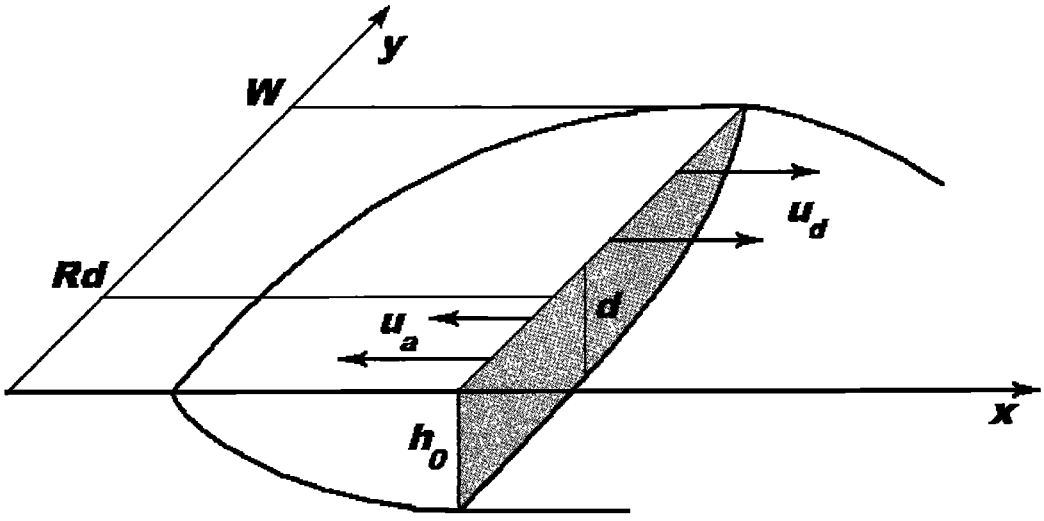

Figure 7. Schematic of alongshelf velocity in the anticyclonic bulge.

coastal wall at x=90-100 km. Finally, from day 12.5 through day 15, during high and increasing runoff, the bulge again grows predominantly in its downstream part while the upstream position of the front remains unchanged. In the downstream part the gap between the bulge and the downstream coastal current is filled with buoyant water, and the secondary bulge reaches its maximum offshore extension. Thus, under conditions of low runoff the anticyclone's flow field controls the source region dynamics and drives the buoyant discharge first upstream and then around the bulge. In the downstream segment of the anticyclone, heavier water flows toward the coast and then upstream along the wall causing the retreat of buoyant water back to the coast and producing a partly detached plume. Strong discharge suppresses the anticyclone's circulation: The flow turns immediately downstream upon entering the model domain. This causes a maximum growth in the downstream part of the bulge, while the upstream part is relatively unchanged.

A partially detached plume is formed when discharge subsides (Figures 5 and 6). The bulge is deformed from an almost circular, azimuthally symmetric form to one swept or tilted downstream. Figure 6 shows that the location of maximum offshore extension of the plume indeed shifts downstream from day 5 through 10 (marked with the triangles). Concurrently, the plume advances upstream from the mouth. Maximum upstream penetration occurs at the offshore distance of *Rd*. As a result, the frontal zone of the upstream half of the bulge on day 10 forms an angle pointing upstream.

We illustrate this deformation of the plume after the high-runoff event using the following argument. The plume is approximated as a buoyant layer of thickness d with density anomaly ρ separated from the quiescent ambient water by an infinitesimal interface. There is no recirculation at the time the discharge peaks: All flow propagates downstream within the bulge (Figure 5, day 15). Since the across-shelf momentum balance is approximately geostrophic at the location of maximum offshore extension (as our model results demonstrate), the absence of recirculation implies that d decreases monotonically offshore from h_0 at the coastal wall. Now assume that the discharge ceases abruptly. The adjustment of the anticyclonic bulge occurs on two scales: fast adjustment of the order of the inertial period, and slow adjustment associated with the advection of buoyancy.

Let us consider the alongshelf flow in the bulge after the fast adjustment is complete, ignoring time derivative terms associated with the slow adjustment. The downstream velocity through the shaded transect shown in Figure 7 is in geostrophic balance with the across-shelf pressure gradient: $u_d = -g' d_y / f$. Thus the total downstream transport Q_d at the location of the bulge's maximum width W is

$$Q_d = \int_0^W u_d \, dy = \frac{g' h_0^2}{2f}. \tag{9}$$

No geostrophic upstream transport occurs at this stage because the buoyant layer's thickness decreases offshore monotonically as a result of the peak discharge. The upstream transport can be driven only by the alongshelf pressure gradient in the upstream part of the bulge. We ignore frictional effects and recall that the Coriolis term is negligible in the alongshelf momentum balance near the coastal wall [*Gill*, 1982]. Accordingly, the alongshelf momentum balance within a baroclinic Rossby radius of the coast can be written

$$u u_x = -g' d_x \quad (y<Rd). \tag{10}$$

Further offshore ($y \geq Rd$), the Coriolis term becomes important, and the alongshelf pressure gradient will force across-shelf flow. We estimate this upstream ageostrophic transport at the same location as the plume's maximum offshore extension. At the coastal wall the continuity equation yields $u_x = -u d_x / d$. Here we ignore v because of the boundary condition and v_y because the streamlines tend to be parallel to the coast at this location. After substitution in (10), this gives an estimate of u_a (Figure 7):

$$u_a = -\sqrt{g' h_0} \quad (y=0), \quad u_a = 0 \quad (y=Rd). \tag{11}$$

The total upstream transport is $Q_u = R d h_0 u_a(x_a, 0)/2 = -g' h_0^2 / (2f)$. Hence the absolute values of the downstream

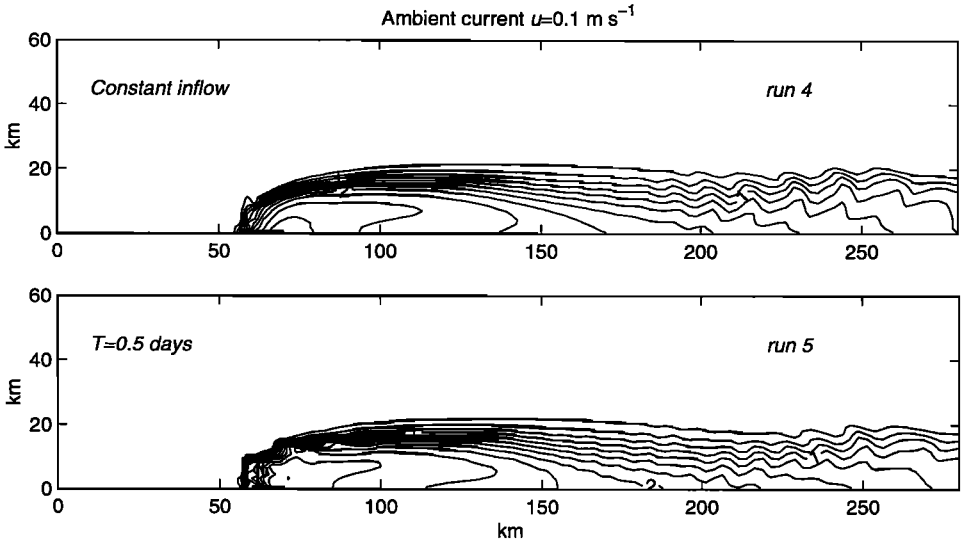

Figure 8. As in Figure 4 but for model runs 4 and 5, day 20.

and upstream transports are equal, and the anticyclonic bulge therefore maintains its alongshelf position. The width W of the bulge is typically several Rd [*Yankovsky and Chapman*, 1997]. As a result, the downstream flow is broad, but the upstream flow occupies only a fraction of the bulge width, concentrating its transport near the coastal wall. This alters the semicircular shape of the bulge formed by maximum discharge. The more energetic and localized upstream flow forms a "nose" at the upstream edge of the bulge near the coast. The wider and slower downstream flow shifts the location of the maximum offshore plume extension slightly downstream. This pattern is clearly seen both in Figure 4 (bottom) and in Figure 6 between days 5 and 10.

3.2. Harmonic Buoyant Inflow in the Presence of a Uniform Downstream Flow

The dynamics and structure of the anticyclonic bulge are highly sensitive to the presence of an ambient coastal current [*Fong*, 1998]. For this reason, we repeat the three previous cases with a specified uniform alongshelf flow of 0.1 m s^{-1} in the downstream direction. Figure 8 shows the resulting density fields on day 20 for the case of constant inflow (model run 4, Figure 8, top) and the inflow varying at the tidal frequency (model run 5, Figure 8, bottom). As in cases without the ambient flow, the spatial structure of the plume is similar. An ambient current impedes the offshore growth of the buoyant bulge so that the bulge is elongated in the downstream direction as far as x=150 km. By day 20 the buoyant flow has reached a steady state near the source region (or periodic in the case of variable inflow), while the flow field still continues to evolve downstream of the bulge (x>150 km).

When the inflow varies at the subinertial frequency (10 day period, model run 6), anticyclones periodically detach from the source following the 10 day cycle of the buoyant inflow (Figure 9). The anticyclones subsequently drift downstream and gradually mix with the buoyant water. However, even after detachment from their source the anticyclones continue to change their configuration because of the variable discharge. They almost disappear on days 20 and 30, when the discharge ceases, but are well pronounced on days 15 and 25, when the discharge is maximum. The anticyclones are observed at x=120-180 km, i.e., at the downstream edge of the primary bulge attached to the mouth, and evolve in a manner similar to the secondary bulge in model run 3 with subinertial harmonic discharge. When the buoyant flow subsides, an anticyclone is advected downstream from its source by the ambient current. At the same time, closed circulation forms around the pool of lightest water in this anticyclone. This closed flow pattern persists until a new pulse of downstream flow is forced by the next discharge peak. The downstream flow converges with the anticyclone's upstream flow near the coastal wall. This convergence shifts the anticyclone slightly offshore and makes it a pronounced feature for a short period of time. As high runoff continues, the density field is smoothed in the alongshelf direction and the anticyclone vanishes.

A mean current arrests the continuous growth of the anticyclonic bulge. Therefore the buoyancy-driven current can achieve either a steady state or a purely periodic regime, depending on the type of inflow. Periodic behavior is clearly seen in Figure10: Density contours representing different times but the same phase of discharge variability (i.e., days 15 and 25 or 10, 20, and 30) coincide near the source region. The area of pure periodic behavior gradually expands downstream extending to x=170 km by day 30: The density contour corresponding to day 30 overlaps its counterpart for day 20 from the source over the alongshelf distance x~170 km. Pure periodic behavior of the buoyancy-driven current demonstrates that the anticyclones in Figure 9 do not result from the development of unstable exponentially growing modes. The latter mechanism is usually invoked to explain such mesoscale features. Instead, the interplay of subinertially varying discharge and the ambient shelf current is responsible for this rich mesoscale flow field.

3.3. Individual Pulse of Buoyant Discharge

In all previous cases, the variability of buoyant discharge was represented in a highly idealized way. This was especially true for the subinertial variability, which in the

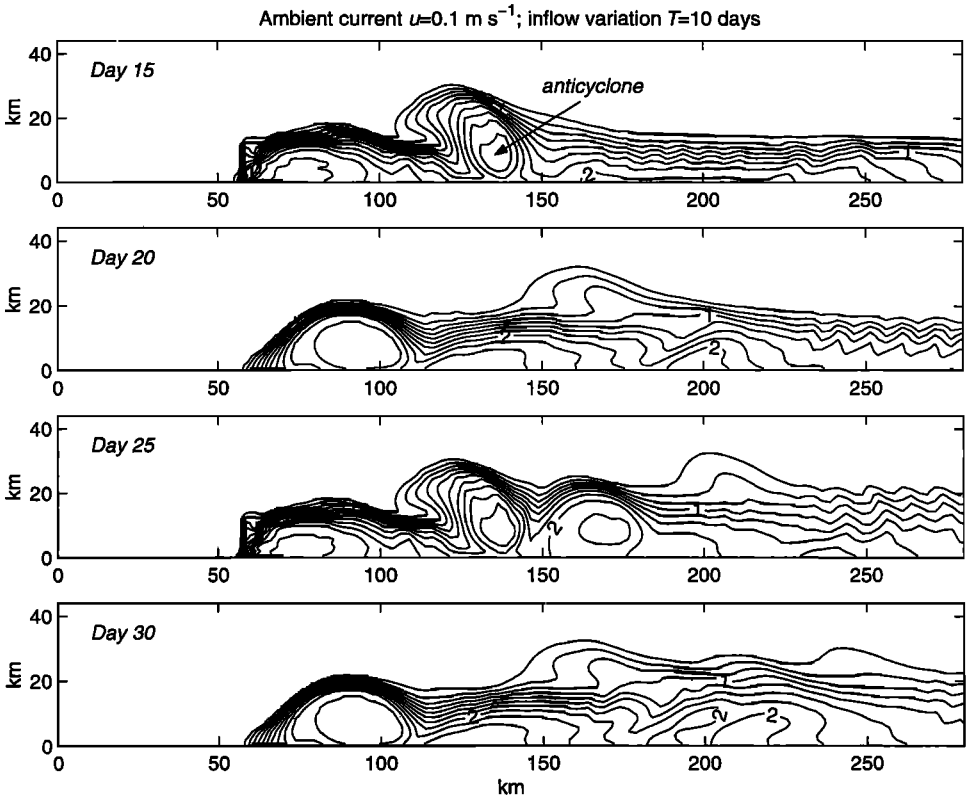

Figure 9. As in Figure 4 but for model run 6, from day 15 to day 30.

real ocean is rarely periodic and almost never drops to zero. In the next three runs we will consider an individual event as a pulse in the buoyant discharge. When the riverine discharge increases, the estuarine buoyant discharge at the mouth is characterized by both a higher volume transport and a greater density anomaly [*Münchow and Garvine*, 1993]. Therefore we introduce a 5 day pulse in buoyant forcing as

$$v_i = 0.1+0.2\sin^2[\omega(t-t_0)] \quad \rho_i = -2-3\sin^2[\omega(t-t_0)]$$

$$5<t<10 \text{ days} \qquad (12)$$

where ω=7.272 10^{-6} s^{-1} (i.e., 10 day period) and t_0=5 days. Otherwise, v_i and ρ_i are held constant with corresponding values set to 0.1 m s^{-1} and –2 kg m^{-3}. The model is first run without ambient flow dynamics (model run 7). Figure 11 shows a sequence of surface density fields near the source region along with contours of the corresponding integral streamfunction. At the time of maximum discharge (7.5 days) a semicircular bulge has formed with all buoyant water flowing downstream and no closed streamlines. The situation is similar to the previous case with subinertial harmonic inflow. Thus the lightest water appears downstream of the mouth. When the discharge and density anomaly subside, a closed anticyclonic circulation develops around the pool of lightest water (Figure 11, day 10). The center of this pool is ~10 km downstream from the mouth, and the bulge has a maximum width at this location. The anticyclonic bulge has a downstream-swept shape as in model run 3 with subinertial harmonic inflow. The –1.0 kg m^{-3} density anomaly contour is shown in Figure 11 to emphasize this pattern. However, the lightest water does not detach from the coast because the closed circulation around the anticyclone quickly decays (compare days 10 and 15 in Figure 11). This anticyclone slowly drifts downstream at ~1.2 km d^{-1}. Mixing gradually reduces its density contrast, and the emerging buoyant inflow fills the upstream part of the bulge. The semicircular shape of the bulge is thus restored by day 20 (not shown).

Although the variations of both inflow velocity and

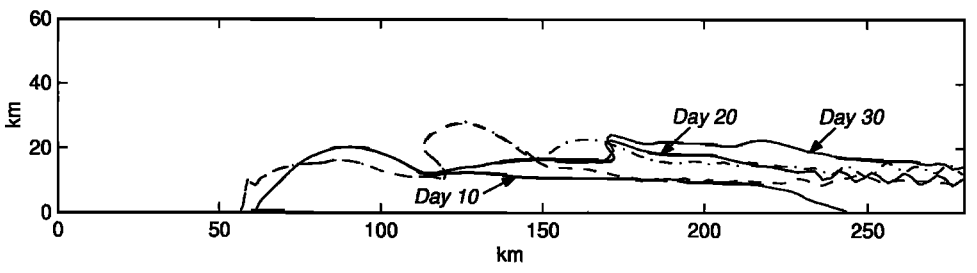

Figure 10. As in Figure 6 but for model run 6 at 5 day intervals from day 10 through day 30. Solid lines are days 10, 20, and 30; dashed line is day 15; dash-dotted line is day 25.

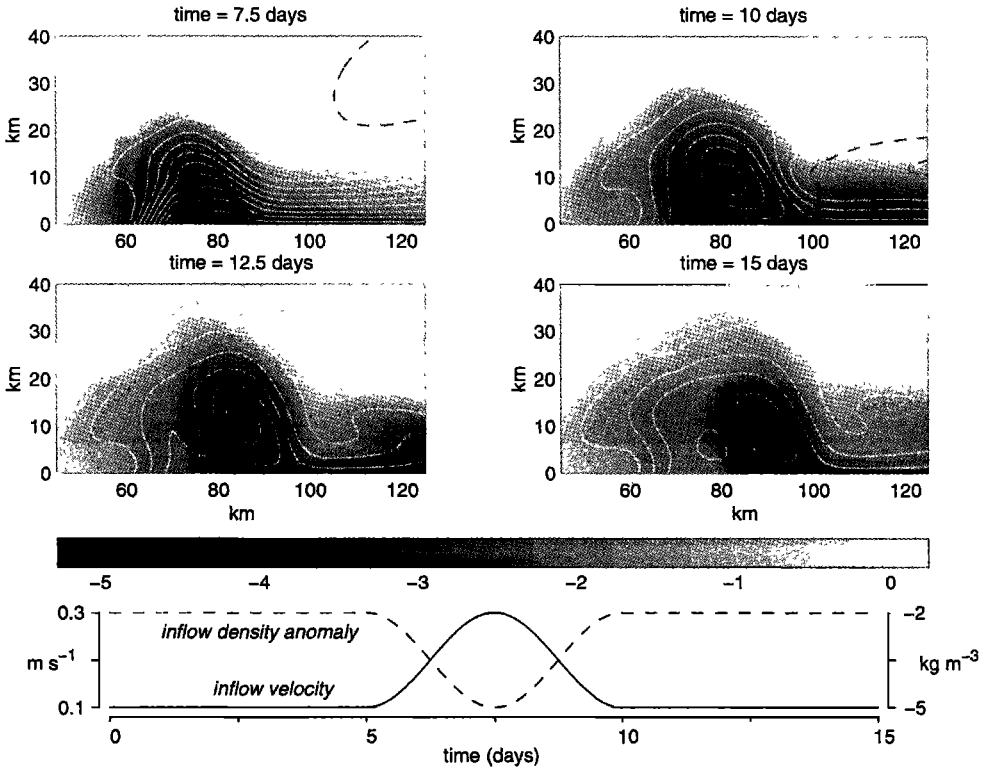

Figure 11. As in Figure 5 but for model run 7. The dotted line is the density contour −1 kg m^{-3}. The bottom diagram shows the temporal evolution of the inflow velocity and the density anomaly.

density anomaly in model run 7 were significant, the duration of the event was rather short. For this reason, in model run 8 we extend the duration of the discharge pulse to 10 days (from day 5 through day 15) with the frequency ω in (12) reduced by half. The surface density fields of model runs 7 and 8 are compared in Figure 12. Both fields are shown 5 days after the discharge has subsided to its background level, on day 15 in model run 7 and on day 20 in model run 8. The anticyclone resulting from the inflow pulse is stronger in model run 8 than in run 7. The lightest water is now separated from the coast. The bulge is wider and its maximum offshore extension is shifted farther downstream than in model run 7. This plume is similar to the partially detached plume in model run 3, except that now the lightest water is completely separated from the source because of the variations in inflow density anomaly.

As the comparison between model runs 7 and 8 indicates, an increase in pulse duration produces a stronger response in the bulge's dynamics and structure. However, this trend cannot be extrapolated to significantly longer periods. When the duration of a pulse is increased still farther, the rate of inflow variability can fall below the intrinsic rate of bulge

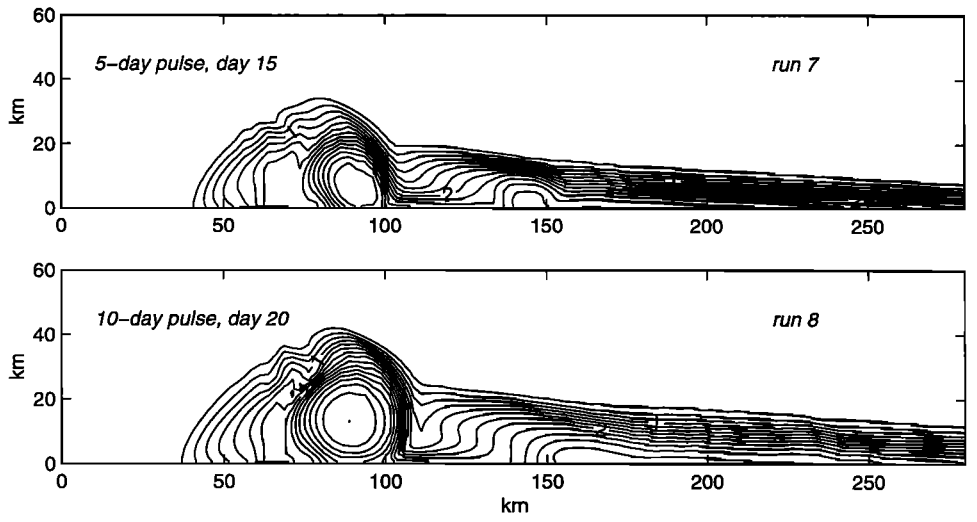

Figure 12. As in Figure 4 but for model run 7, day 15, and model run 8, day 20.

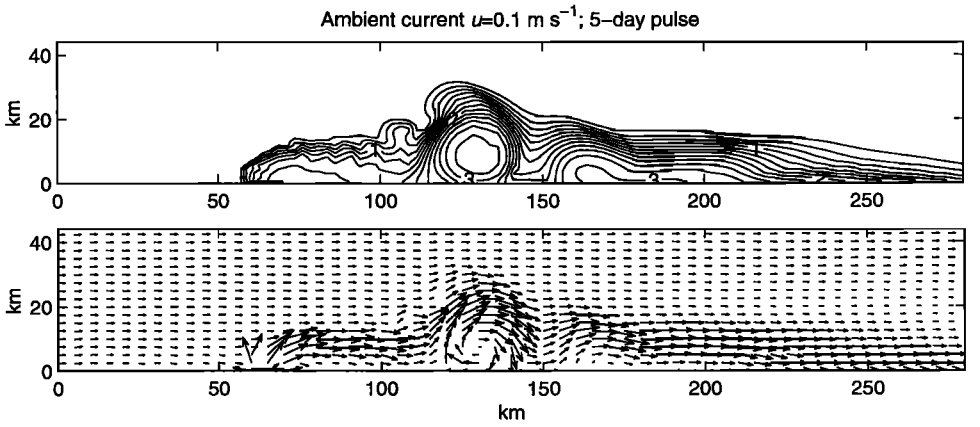

Figure 13. Model run 9, day 15: (top) absolute value of the density anomaly at the surface with a contour interval of 0.25 kg/m^3, and (bottom) velocity at the surface. Scale for the velocity vector is 0.1 m s^{-1} at the upstream boundary.

growth occurring even under conditions of constant inflow (Figure 3, bottom). Thus the impact of inflow variability will be masked by the unbounded growth of the bulge. Because the latter tendency is not strongly supported by observations [*Garvine*, 2001], we will not elaborate on low-frequency limit for inflow variability.

The effect of a discharge pulse is more dramatic when an ambient alongshelf current of 0.1 m s^{-1} is added (Figure 13). In this case the anticyclone is advected downstream by the ambient current. It maintains its almost circular shape with an anticyclonic flow pattern because it contains lighter water than the surrounding buoyant flow. The frontal zone of the

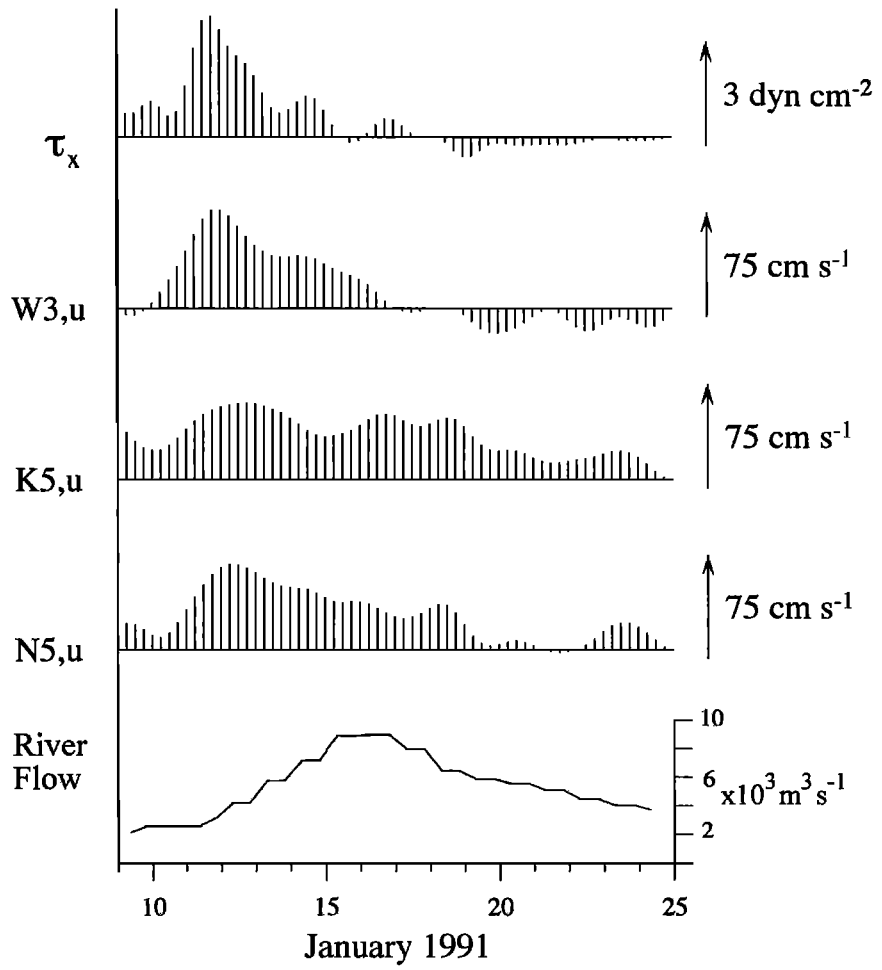

Figure 14. Time series of (top to bottom) low-pass filtered alongshelf wind stress and currents at 10 m measured at moorings W3, K5, and N5 (mooring locations are shown in Figure 15) and daily river flow into the Columbia estuary. Velocity is positive downstream (northward).

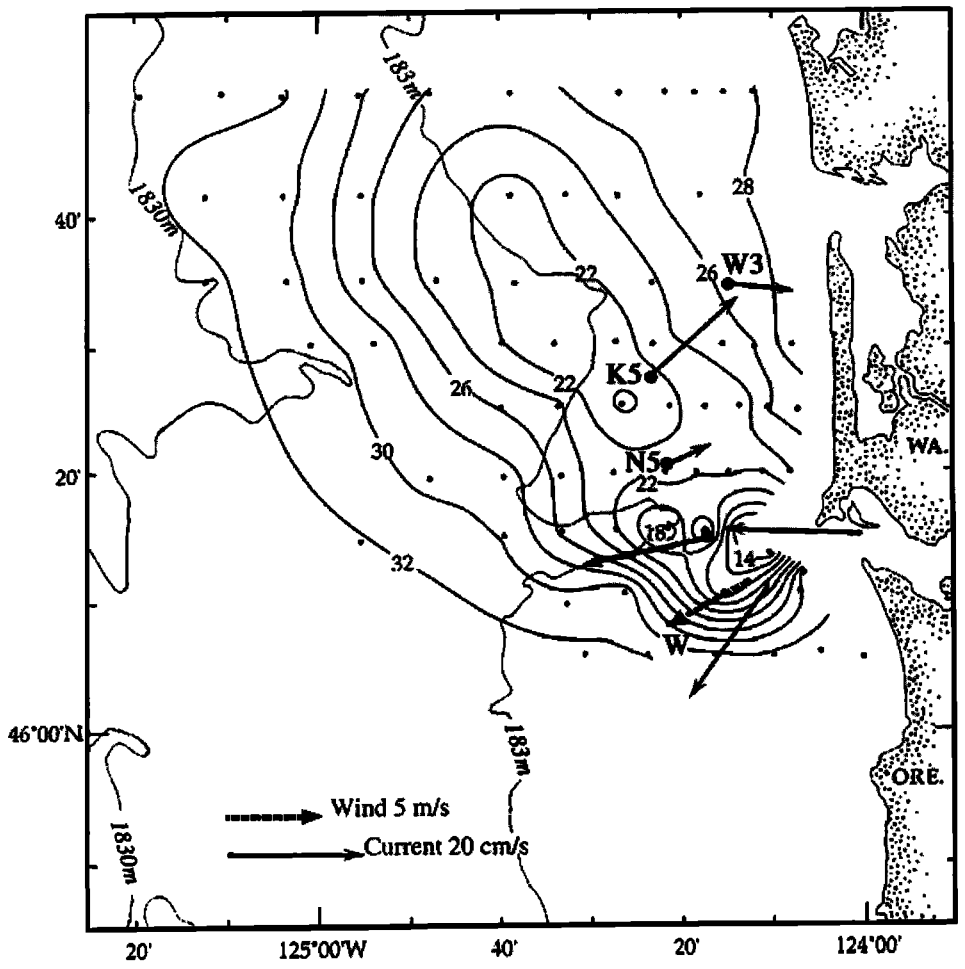

Figure 15. Columbia River plume. Salinity (psu) map at 1 m obtained on January 20-22, 1991. Also shown are low-pass filtered currents from moorings at 5 m depth at the times of nearby CTD casts and the wind vector W averaged over the duration of the survey.

buoyant current has an abrupt offshore excursion adjacent to this anticyclone. Interestingly, while constant buoyant inflow in the presence of a mean current produces an elongated plume with almost no bulge (Figure 8), variable discharge in the presence of a mean current generates almost circular anticyclonic bulges during periods of maximum discharge.

4. Observational Examples

In this section we discuss two observational examples of buoyant plumes formed under conditions of time-variable discharge. One example was obtained from the source region of the Columbia River plume; the other describes the downstream region of the Hudson Coastal Current along the New Jersey coast.

4.1. Columbia River Plume

Observations of the Columbia River plume were obtained from October 1990 to April 1991 [*Hickey et al.*, 1998]. To date, this is one of the most comprehensive observational studies of buoyant coastal plumes. The observations included several shipboard surveys covering the anticyclonic bulge near the source as well as time series from moorings. Data collected on January 20-22, 1991, are particularly valuable for our study. The conditions preceding the formation of the anticyclonic bulge observed on January 20-22 are summarized in Figure 14. Figure 14 shows low-pass filtered time series of alongshelf wind stress and 10 m currents measured from the moored buoys along with daily averaged river discharge into the Columbia estuary. A strong wind event on January 11-14 generated northward, i.e., downstream flow, just prior to a strong discharge event. The northward flow, which exceeded 0.5 m s^{-1}, probably advected downstream and mixed any preexisting anticyclonic bulge in the source region. Thus this storm cleared the way for the arrival of a new discharge pulse on January 15-17. The maximum discharge exceeded 9000 m^3 s^{-1}, more than triple the discharge on January 10. The discharge gradually subsided to <6000 m^3 s^{-1} during the survey, while wind forcing and resulting wind driven currents were both weak. The 10 m currents shown in Figure 14 can be considered as ambient shelf currents since the plume was very shallow during the January 20-22 survey period [*Hickey et al.*, 1998, Figure 6).

The surface salinity field as well as low-pass filtered current vectors at 5 m at the times nearest to those of nearby conductivity-temperature-depth (CTD) casts are shown in Figure 15. As in the model runs with variable discharge, the

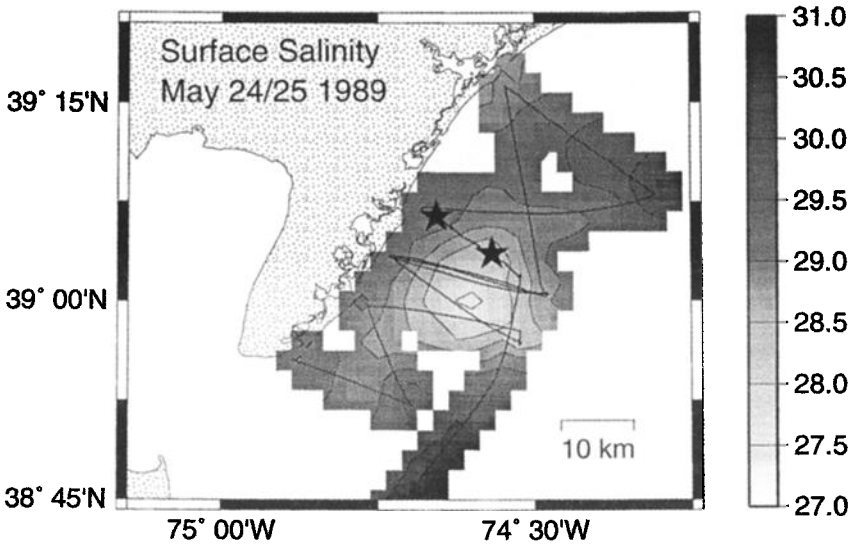

Figure 16. Southern New Jersey shelf. The surface salinity map was obtained from 1800 UTC May 24 through 1000 UTC May 25, 1989. Ship track and mooring locations (solid stars) are also shown.

buoyant water forms a partially detached bulge with maximum offshore extension approximately 35-40 km downstream from the source depending on the choice of salinity contour. The lightest water is separated from the coast. A closed contour of 22 practical salinity units (psu) occurs offshore and downstream from the source. This pool of relatively fresh water is likely a result of the Columbia River peak discharge event on January 15-17. The horizontal structure of the Columbia River plume is qualitatively similar to the pattern in model run 8 (Figure 12), except that the lightest water is observed at the mouth, rather than in the downstream section of the bulge formed under maximum runoff conditions. This is not surprising because the Columbia River plume is thin (5-10 m thick) and is exposed to significant vertical mixing by wind and tidal forcing. The patchy structure of the salinity field near the mouth is likely caused by the tidal variability of the inflow. These features have a spatial scale of several kilometers and tend to disappear some distance from the mouth as in model run 2 (Figure 4).

Available velocity vectors at 5 m during the survey are also consistent with patterns derived from the model runs (Figure 15). This is especially true for cross-shelf velocity. In the upstream "corner" of the bulge, adjacent to the mouth, strong offshore currents (15-20 cm s^{-1}) were observed, while measurements in the downstream/coastal segment of the bulge consistently showed onshore currents (Figure 15). The alongshelf component, on the other hand, does not represent plume dynamics solely; in particular it contains a wind-driven component: Ekman transport associated with the offshore wind stress as well as the current accelerated alongshore by the weak alongshore wind stress.

4.2. Hudson Coastal Current

Observations of a buoyancy-driven coastal current originating from the Hudson River discharge and propagating along the New Jersey coast in May – June 1989 were described by *Münchow* [1992]. The measurement site is ~150 km downstream of the estuary mouth. For this

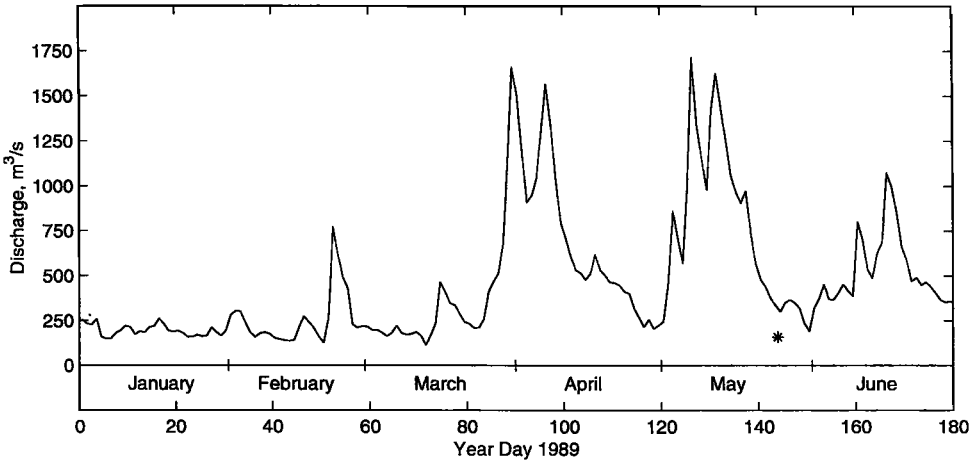

Figure 17. Temporal evolution of daily Hudson River discharge at Greenville, New York. Asterisk shows the date of the shipboard survey.

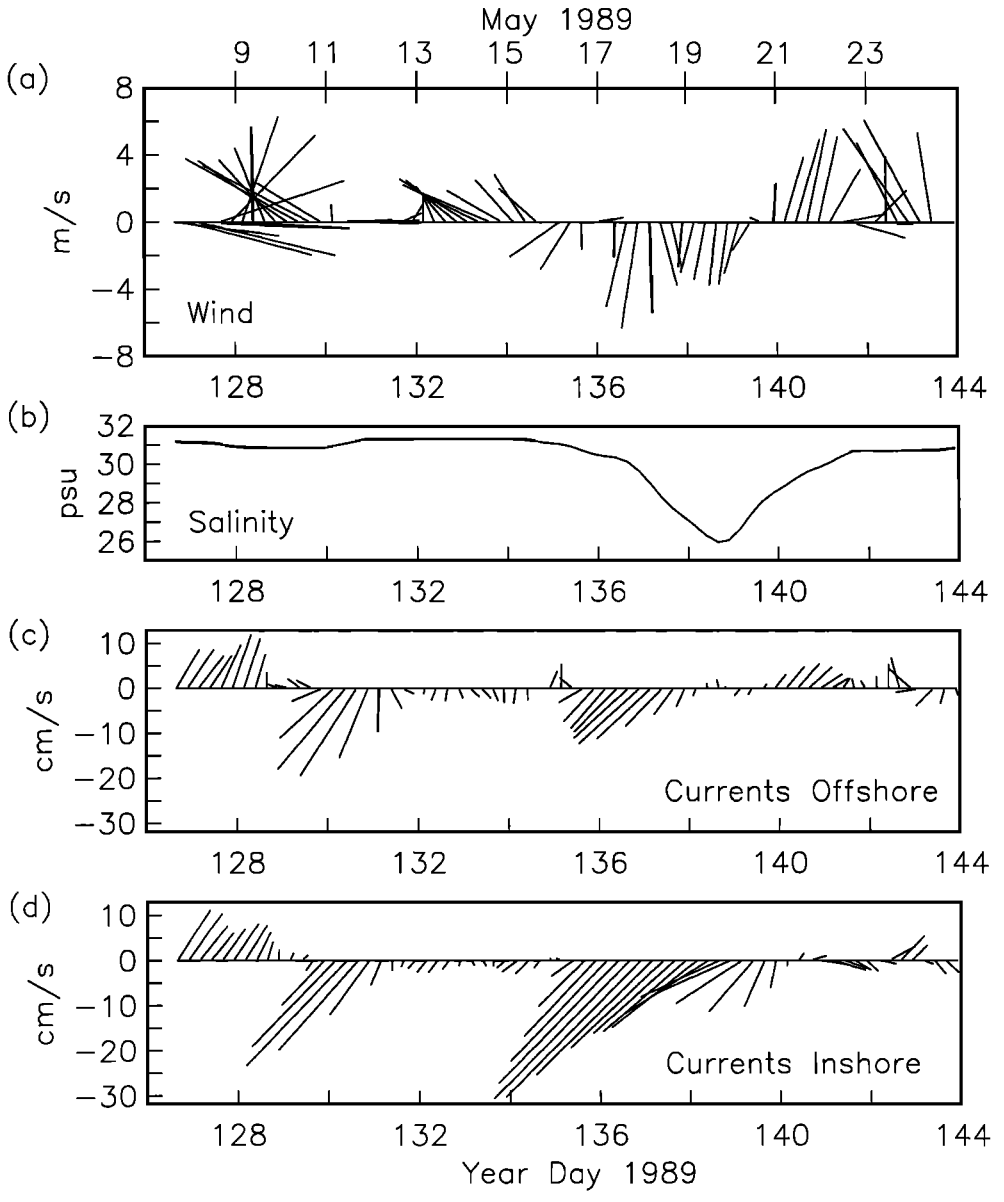

Figure 18. Time series of low-pass filtered (a) wind, (b) salinity, (c) currents at offshore, and (d) inshore moorings. Mooring locations are shown in Figure 16.

alongshelf distance one might expect only a moderate signature of the buoyant waters in the study area. However, a striking finding in the data was the episodic arrival and southward advection of intense anticyclonic eddies. An example from May 24-25 is shown in Figure 16. The anticyclone is remarkably similar to its model counterpart in Figure 13 which was produced by discharge pulse and was advected downstream from the buoyancy source by the mean current. Indeed, the shelf near the coast is filled with buoyant water of 29-29.5 psu, while the salinity of the ambient water is 30-31 psu, and the anticyclone with minimum salinity of 27.5 psu is imbedded in the coastal buoyant flow. The center of the anticyclone is shifted offshore from the coast with a frontal zone between the core and the coastline. The spatial scale of the eddy (~20 km) is also consistent with model results (Figure 13).

Figure 17 shows that time-dependent buoyancy forcing was consistent with the formation of the anticyclonic eddy in Figure 16. The Hudson River streamflow had two events of high discharge prior to the observations: year days 85-100 and 125-140. These streamflow data were obtained from the freshwater gauge at Greenville, New York, located ~250 km upstream from the mouth of the Hudson estuary. *Münchow* [1992] argued for a 7 week time lag between the peak discharge at Greenville, New York, and the arrival of buoyant waters at the site of these observations. *Yankovsky and Garvine* [1998] also found a time lag of more than 1 month between the observations of high discharge at the Hudson River gauge and the arrival of low-salinity waters off the New Jersey coast 100 km downstream from the mouth in summer 1996. Thus the first discharge event near year days 85-100 (Figure 17) is likely responsible for the generation of the anticyclone observed on May 24-25 (year days 143-144). Wind forcing in this region during summer is generally upwelling–favorable. However, just before the low-salinity event downwelling-favorable winds persisted

for several days (May 16-20, Figure 18a) facilitating the development of a downstream current as observed in the mooring records, with higher velocity at the inshore location (Figures 18c and 18d). Salinity 6 m below the surface at the inshore mooring drops by 5 psu from May 16 to May 20. At the time of the shipboard measurements shown in Figure 16 (May 24 –25) the eddy has nearly passed the mooring line. We infer that this lower salinity was associated with the high river runoff in the Hudson estuary consistent with the mechanism described in our model results, namely, a pulsed discharge in the presence of downstream ambient flow.

5. Discussion and Summary

Our results show that time-variable discharge at subinertial frequency modifies the dynamics of a buoyant coastal plume compared with the buoyant plume formed with the same amount of buoyant water discharged at a constant rate. A partially detached anticyclonic plume forms when the discharge subsides after reaching its peak value. Such a plume has a maximum offshore extension some distance downstream of the river mouth, and the lightest water at this location is separated from the coast. When discharge is higher than the average, the inflow turns downstream, and the bulge grows in its downstream segment. When discharge is low, a closed anticyclonic circulation develops around the bulge. This anticyclonic eddy dominates the dynamics in the source region: It advects newly discharged water upstream and offshore around the bulge. Concurrently, it carries heavier ambient water toward the coast along the downstream edge of the bulge. A secondary bulge or anticyclone forms during the low-runoff interval. When high discharge resumes, it shifts this anticyclone offshore and makes it pronounced for some time, until it is mixed with the newly arriving buoyant current. Tidal (12 hour period) variability of the inflow, on the other hand, has little impact on the buoyant plume.

We introduced the variability of buoyant inflow both as harmonic fluctuations of the inflow rate and as an individual pulse of higher runoff with greater density anomaly. Indeed, river water often discharges into an estuary and reaches the coastal ocean only after substantial mixing with oceanic water that has entered the estuary as a compensating return flow. Increased river runoff will lead to both a higher volume transport of buoyant water at the estuary mouth and a stronger density anomaly. An individual event of higher runoff with stronger density anomaly also generates a partly detached plume after the discharge subsides to its background value. In this case, however, the lightest water occupying the downstream part of the bulge is separated not only from the coast but also from the source. This separation is caused by the limited duration of the lightest water runoff.

The impact of discharge variation becomes more dramatic when an ambient shelf circulation is added. For simplicity, we introduced only a uniform steady downstream flow. Both constant and tidally varying discharges in the presence of an ambient current produce an elongated plume with almost no bulge. On the other hand, subinertial variability of the inflow generates an almost circular bulge during high runoff. Subsequently, this bulge separates from the source and either continues to propagate downstream as an individual eddy advected by the ambient current or is modified by the next cycle of high discharge. This cycling produces anticyclones downstream from the newly formed bulge at the source. The effect of pulsed discharge can thus explain why pronounced anticyclonic bulges are observed in nature, even though ambient currents are ubiquitous on continental shelves. In this study, we focused on the case of a downstream mean current since weak upstream flow causes periodic shedding of anticyclones even with constant discharge [*Yankovsky*, 2000].

Our model experiments represent a process-oriented study and as such are not designed to reproduce specific coastal buoyant systems. Instead, the model configuration is simplified in order to make the interpretation of one specific process, the effect of time-variable discharge, more straightforward. This approach has limitations; for example, the dynamics in the estuary mouth are not properly resolved: Spatially uniform discharge through a rectangular gap in the coastal wall is utilized. This simplification assumes that the structure of buoyant inflow is only important near the mouth. Such a simplification can be justified for our examples in which inflow velocities are relatively weak (both Froude and Rossby numbers are well below 1). However, for more energetic discharges the buoyant inflow should be introduced in a more realistic manner.

In this study, we also present observational evidence for both a partially detached anticyclonic bulge near the mouth and an anticyclone propagating downstream from its source. The first feature was observed offshore of the Columbia River estuary in January, 1991, the second feature was observed 150 km downstream of the Hudson River estuary in May 1989. The Columbia River plume on January 20-22, 1991, was swept downstream with its maximum width ~35 km downstream from the source. At this location the lightest water was detached from the coast. A similar structure was observed in an EOF analysis of the 1 m depth salinity time series over a 4 week period [*Hickey et al.*, 1998]. Pulsed discharge occurs frequently from the Columbia River [*Hickey et al.*, Figure 1] favoring the repeated formation of a partly detached plume. We argue that this structure results from the intrinsic plume dynamics, rather than because of the wind forcing. The upwelling-favorable wind can spread the plume offshore and cause its partial separation from the coast. However, it also generates upstream flow, making the downstream-swept structure of the plume very unlikely. Indeed, under conditions of upwelling-favorable wind forcing, the maximum offshore extension of the Columbia River plume occurred near the mouth, not 35 km downstream (*Hickey et al.* [1998], Figure 5b, February 24; and Figure 8, November 26-28).

Off New Jersey the anticyclone with low-salinity water in its center originated from the Hudson estuary ~150 km upstream [*Münchow*, 1992]. As our numerical results show, the generation of such an anticyclone can result from the variability of buoyant discharge in the presence of downstream flow. The presence of anticyclone does not require that the buoyancy-driven coastal current become unstable.

Observational studies in shelf regions affected by buoyant plumes generally show that the subinertial alongshelf component of the current correlates with the wind forcing [e.g., *Hickey et al.*, 1998; *Yankovsky and Garvine*, 1998; *Münchow and Chant*, 2000]. However, *Yankovsky et al.* [2000] showed that strong across-shelf currents on the inner New Jersey shelf were generated at the leading edge of the

arriving buoyant bulge. Similarly, enhanced across-shelf currents were found within the bulge of the Columbia River plume [*Hickey et al.*, 1998, section 5.3 and Figure 17). Thus the presence of buoyant bulges in coastal waters produces energetic and spatially localized across-shelf currents. Our numerical experiments show that for constant buoyant discharge even weak ambient shelf flow tends to suppress the formation of these bulges, producing elongated buoyant plumes instead. On the other hand, almost circular anticyclones are easily formed when the discharge varies at a subinertial frequency. We conclude that subinertial variability of buoyant discharges plays a major role in the generation of a three-dimensional density field in coastal waters with resulting enhanced across-shelf currents.

Acknowledgments. We thank Rich Garvine for helpful comments and discussions. Two anonymous reviewers provided valuable criticism and suggestions. A.Y. was supported by National Science Foundation (NSF) grant OCE-9907995; B.H. was supported by NSF grant OCE-9618186 and NOAA grant NA960P0238-PNCRS; A.M. was supported by NSF grant OCE-0002375.

References

Brink, K. H., Coastal-trapped waves and wind-driven currents over the continental shelf, *Annu. Rev. Fluid Mech.*, *23*, 389-412, 1991.

Chao, S.-Y., River-forced estuarine plumes, *J. Phys. Oceanogr.*, *18*, 72-88, 1988.

Chao, S.-Y., and W. C. Boicourt, Onset of estuarine plumes, *J. Phys. Oceanogr.*, *16*, 2137-2149, 1986.

Chapman, D. C., 2000. Boundary layer control of buoyant coastal currents and the establishment of a shelfbreak front. J. Phys. Oceanogr., 30, 2941-2955.

Chapman, D. C., and S. J. Lentz, Trapping of a coastal density front by the bottom boundary layer, *J. Phys. Oceanogr.*, *24*, 1464-1479, 1994.

Fong, D. A., Dynamics of freshwater plumes: Observations and numerical modeling of the wind-forced response and alongshore freshwater transport, Ph.D. dissertation, 172 pp., Mass Inst. of Technol.-Woods Hole Oceanogr. Inst., 1998.

Garvine, R. W., A dynamical system for classifying buoyant coastal discharges, *Cont. Shelf. Res.*, *15*, 1585-1596, 1995.

Garvine, R. W., Penetration of buoyant coastal discharge onto the continental shelf: A numerical model experiment, *J. Phys. Oceanogr.*, *29*, 1892-1909, 1999.

Garvine, R. W., The impact of model configuration in studies of buoyant coastal discharge, *J. Marine Res.*, *59*, 193-225, 2001.

Gill, A. E., *Atmosphere-Ocean Dynamics*, 662 pp., Academic, San Diego, Calif., 1982.

Haidvogel, D. B., J. L. Wilkin, and R. Young, A semi-spectral primitive equation ocean circulation model using vertical sigma and orthogonal curvilinear horizontal coordinates, *J. Comput. Phys.*, *94*, 151-185, 1991.

Hickey, B. M., L. J. Pietrafesa, D. A. Jay, and W. C. Boicourt, The Columbia River plume study: Subtidal variability in the velocity and salinity fields, *J. Geophys. Res.*, *103*, 10,339-10,368, 1998.

Kourafalou, V. H., L.-Y. Oey, J. D. Wang, and T. N. Lee, The fate of river discharge on the continental shelf, 1, Modeling the river plume and inner shelf coastal current, *J. Geophys. Res.*, *101*, 3415-3434, 1996.

Masson, D., and P. Cummins, Numerical simulation of a buoyancy-driven coastal countercurrent off Vancouver Island, *J. Phys. Oceanogr.*, *29*, 418-435, 1999.

Mellor, G. L., and T. Yamada, A hierarchy of turbulence closure models for planetary boundary layers, *J. Atmos. Sci.*, *31*, 1791-1806, 1974.

Münchow, A., The formation of a buoyancy driven coastal current, Ph.D. dissertation, 205 pp., Univ. of Del., 1992.

Münchow, A., and R. J. Chant, Kinematics of inner shelf motions during the summer stratified season off New Jersey, *J. Phys. Oceanogr.*, *30*, 247-268, 2000.

Münchow, A., and R. W. Garvine, Dynamical properties of a buoyancy driven coastal current, *J. Geophys. Res.*, *98*, 20,063-20,077, 1993.

Nof, D., and T. Pichevin, The ballooning of outflows, *J. Phys. Oceanogr.*, in press, 2001.

Oey, L.-Y., and G. L. Mellor, Subtidal variability of estuarine outflow, plume, and coastal current: A model study, *J. Phys. Oceanogr.*, *23*, 164-171, 1993.

Pichevin, T., and D. Nof, The momentum imbalance paradox, *Tellus*, *49A*, 298-319, 1997.

Simpson, J. H., and A. J. Souza, Semidiurnal switching of stratification in the region of freshwater influence of the Rhine, *J. Geophys. Res.*, *100*, 7037-7044, 1995.

Song, Y., and D. Haidvogel, A semi-implicit ocean circulation model using a generalized topography-following coordinate system, *J. Comput. Phys.*, *115*, 228-244, 1994.

Sugimoto, T., A review of recent physical investigations on the straits around the Japanese Islands, in *The Physical Oceanography of Sea Straits, NATO Sci. Ser., Ser. C*, vol. 318, edited by L. J. Pratt, pp. 191-209, Kluwer Acad., Norwll, Mass., 1990.

Valle-Levinson, A., J. M. Klinck, and G. H. Wheless, Inflows/outflows at the transition between a coastal plain estuary and the coastal ocean, *Cont. Shelf Res.*, *16*, 1819-1847, 1996.

Weaver, A. J., and W. W. Hsieh, The influence of buoyancy flux from estuaries on continental shelf circulation, *J. Phys. Oceanogr.*, *17*, 2127-2140, 1987.

Yankovsky, A. E., The cyclonic turning and propagation of buoyant coastal discharge along the shelf, *J. Mar. Res.*, *58*, 585-607, 2000.

Yankovsky, A. E., and D. C. Chapman, A simple theory for the fate of buoyant coastal discharges, *J. Phys. Oceanogr.*, *27*, 1386-1401, 1997.

Yankovsky, A. E, and R. W. Garvine, Subinertial dynamics on the inner New Jersey shelf during the upwelling season, *J. Phys. Oceanogr.*, *28*, 2444-2458, 1998.

Yankovsky, A. E, R. W. Garvine, and A. Münchow, Mesoscale currents on the inner New Jersey shelf driven by the interaction of buoyancy and wind forcing, *J. Phys. Oceanogr.*, *30*, 2214-2230, 2000.

B. M. Hickey, School of Oceanography, University of Washington, Box 357940, Seattle,WA 98195, USA (bhickey@u.washington.edu)

A. K. Münchow, College of Marine Studies, University of Delaware, Newark, DE 19716, USA (muenchow@udel.edu)

A. E. Yankovsky, Nova Southeastern University Oceanographic Center, 8000 North Ocean Drive, Dania Beach, FL 33004, USA (sasha@nova.edu)

(Received January 12, 2001; revised May 23, 2001;
accepted June 4, 2001.)